RGNZ/MGPB

A Novel Approach to Landslide Monitoring based on Unmanned Aerial System Photogrammetry

Rudarsko-geološko-naftni zbornik
(The Mining-Geology-Petroleum Engineering Bulletin)
UDC: 528:551
DOI: 10.17794/rgn.2022.5.8

Original scientific paper

Ivan Jakopec[1,3]; Ante Marendić[1,4]; Igor Grgac[2,5]

[1] *University of Zagreb, Faculty of Geodesy, Kačićeva 26, 10000 Zagreb, Croatia,*
[2] *PNT tech d.o.o., Bukovački obronak 26, 10000 Zagreb, Croatia*
[3] *https://orcid.org/0000-0003-0766-5067 (Ivan Jakopec)*
[4] *https://orcid.org/0000-0003-3524-5262 (Ante Marendić)*
[5] *https://orcid.org/0000-0002-7377-7596 (Igor Grgac)*

Abstract

Landslides represent great dangers that can cause fatalities and huge property damage. To prevent or reduce all possible consequences that landslides cause, it is necessary to know the kinematics of the surface and undersurface sliding masses. Geodetic surveying techniques can be used for landslide monitoring and creating a kinematic model of the landslide. One of the most used surveying techniques for landslide monitoring is the photogrammetric survey by Unmanned Aerial System. The results of the photogrammetric survey are dense point clouds, digital terrain models, and digital orthomosaic maps, where landslide displacements can be determined by comparing these results in two measurement epochs. This paper presents a new data processing method with a novel approach for calculating landslide displacements based on Unmanned Aerial System photogrammetric survey data. The main advantage of the new method is that it does not require the production of dense point clouds, digital terrain models, or digital orthomosaic maps to determine displacements. The applicability and accuracy of the new method were tested in a test field with simulated displacements of known values within the range of 20-40 cm in various directions. The new method successfully determined these displacements with a 3D accuracy of ±1.3 cm.

Keywords:

landslide; monitoring; unmanned aerial systems; structure from motion; photogrammetry

1. Introduction

A landslide is the movement of a mass of rock, earth, or debris down a slope due to disturbances in soil stability (**Cruden, 1991**). Landslides represent significant potential dangers that can cause great material, economic, social, and human losses (**Mihalić Arbanas and Arbanas, 2014**) and are responsible for 9% of all world disasters (**Galli et al., 2008**).

During the winter of 2012 to 2013, more than 900 landslides caused by natural processes were activated in continental Croatia, which caused significant material damage (**Arbanas et al., 2013**). Croatia's largest landslide is Kostanjek, located in the city of Zagreb. As a part of the continuous real-time monitoring system, a series of sensors are installed on the Kostanjek Landslide to acquire information of landslide kinematics to react in time and prevent a potential catastrophe (**Krkač et al., 2021, 2019**). Understanding the behaviour of landslides and identifying their possible triggering effects usually requires good knowledge of the kinematic surface and subsurface sliding masses (**Acar et al., 2008**).

Corresponding author: Ivan Jakopec
e-mail address: ivan.jakopec@geof.unizg.hr

Besides the continuous real-time monitoring system, knowledge about the landslide kinematics can be acquired by many different monitoring techniques, which differ according to the surveying principle. The most conventional monitoring technique is based on classical geodetic surveying using the precise level, total station or GNSS receiver, providing sparse spatial point coverage with very high survey accuracy. It is time-consuming, but it can declare well-defined information about possible displacements and landslide movements (**Afeni and Cawood, 2013; Artese and Perrelli, 2018; Kasperski et al., 2010; Martha et al., 2010; Simeoni et al., 2015; Sui et al., 2008; Tsai et al., 2012**). Optical data acquired from airborne or satellite platforms can be an alternative solution for landslide mapping and monitoring (**Mondini et al., 2011; Nichol and Wong, 2005**), where high-resolution data are very efficient in detecting individual landslides or groups of landslides providing important surface texture data (**Fiorucci et al., 2011; Marcelino et al., 2009; Metternicht et al., 2005**). However, terrain models produced by these techniques are not as accurate and precise as models produced by the Airborne Laser Scanning (ALS) technique (**Baltsavias, 1999**) based on Light Detection And Ranging (LiDAR)

remote sensing technique measured from an aircraft (**Yu et al., 2015**), and it is a powerful tool for the fast collection of large densities of accurate and high spatial resolution of landslides, improving better-analyzing surface topography (**Abellán et al., 2010; Ardizzone et al., 2007; Eeckhaut et al., 2007; Jaboyedoff et al., 2012, 2009; Oppikofer et al., 2008; Tang et al., 2022; Teza et al., 2007**). Still, it is pretty expensive for individual landslide studies (**Westoby et al., 2012**). Lidar measurements can also be performed from the ground by Terrestrial Laser Scanning (TLS), providing a very high survey accuracy which improves a better understanding of changes and deformations of the landslide (**Barbarella and Fiani, 2013; Castagnetti et al., 2014; Luo et al., 2017; Oppikofer et al., 2012; Spreafico et al., 2015**). Still, it can be time-consuming and challenging when dealing with highly steep terrain (**Westoby et al., 2012**). The Synthetic-Aperture Radar (SAR) technique from aircraft or satellite platforms provides a wide coverage area with a high spatial resolution (**Bardi et al., 2017; Bozzano et al., 2017; Du et al., 2017; Kang et al., 2017; Mondini, 2017; Qi et al., 2017; Schlögel et al., 2017; Yang et al., 2017; Zhao and Lu, 2018**). The ability of microwave radar sensors to see through clouds in the presence or absence of daylight makes it a well-suited technique for quickly detecting and mapping individual landslides, landslide populations of different types and sizes over a wide area, and different physiographic characteristics (**Adriano et al., 2020; Aimaiti et al., 2019; Burrows et al., 2019; Ge et al., 2019; Mondini et al., 2021; Park and Lee, 2019**).

In the last few decades, the monitoring technique based on Unmanned Aerial Systems (UAS) photogrammetric surveying in cooperation with Structure from Motion (SfM) and Multi-View Stereo (MVS) image processing algorithms have become a valuable technique for producing various terrain models (**Ai et al., 2015; Eltner et al., 2016; Fraser and Cronk, 2009; James and Robson, 2014, 2012; Passalacqua et al., 2015; Remondino and El-Hakim, 2006; Tarolli, 2014**) and plays a vital role in landslide monitoring tasks (**Clapuyt et al., 2017; Eker et al., 2018; Jakopec et al., 2021; Lin et al., 2010; Lucieer et al., 2014; Marendic et al., 2017; Niethammer et al., 2012; Nikolakopoulos et al., 2017, 2015; Pajares, 2015**). This monitoring technique has become very desirable and affordable due to technological developments such as autopilot systems, lightweight action cameras, miniature GNSS receivers, advances in carbon fiber airframes, and the development of new image processing methodologies based on computer vision (**Lucieer et al., 2014; Nikolakopoulos et al., 2015; Smith et al., 2016**). The monitoring by this technique is based on techniques that quantify the topographic changes between products delivered from the SfM-MVS image processing algorithm.

The most used technique to quantify the topographic changes is based on image correlation techniques, which detect corresponding features or patches in two images by correlating their intensity values to detect topographic changes. Many authors use this technique on georeferenced orthomosaic images produced from different survey epochs to determine horizontal landslide displacement (**Jakopec et al., 2021; Marendic et al., 2017; Niethammer et al., 2012; Peternel et al., 2017; Powers et al., 1996**). One of the most used software that uses image correlation techniques is the Co-registration of Optically Sensed Images and Correlation (COSI-Corr) (**Leprince et al., 2007**), and many authors use it in their research to determine horizontal landslide displacements (**Fernández et al., 2016; Lucieer et al., 2014; Turner et al., 2015**). Furthermore, an often-used straightforward technique is DEM of difference (DoD), which involves subtracting a later digital elevation model from an earlier digital elevation model, highlighting the change in one direction along the vertical axis (**Abellán et al., 2009; Hsieh et al., 2016; Lague et al., 2013; Wheaton et al., 2009**). However, the accuracy of calculated differences relies on the produced digital terrain models (**DiFrancesco et al., 2020**). Therefore, the DoD technique is not very suitable for calculating differences on a geometrically complex terrain with overhanging features and wide arrays of surface orientations, so to improve the DoD precision across some terrain surfaces, segments with similar directions can be grouped for separate analysis, but this can complicate processing and data interpretation (**Barnhart and Crosby, 2013**). Several recent studies have used the DoD technique to analyze landslides (**Fernández et al., 2016; Huang et al., 2017; Peternel et al., 2017; Tanteri et al., 2017**). One of the latest direct point cloud comparison techniques is Multiscale Model-to-Model Cloud Comparison (M3C2). This technique directly compares two point clouds and conducts change detection with minimal manual processing (**Lague et al., 2013**). It is the mostly used in geosciences (**Anders et al., 2020; Benjamin et al., 2016; Bonneau and Hutchinson, 2019; Kromer et al., 2015, 2017; Nourbakhshbeidokhti et al., 2019; Stumpf et al., 2015; van Veen et al., 2017**) and excellently quantifies topographic changes between products generated from UAS photogrammetric survey (**Cook, 2017; Eker et al., 2018; Esposito et al., 2017a, 2017b; James et al., 2017; Warrick et al., 2017**).

All the mentioned techniques compare high-resolution products such as digital orthomosaic maps, digital terrain models, and dense point clouds produced from acquired images in two different UAS photogrammetric survey epochs to quantify the topographic changes (**Eltner et al., 2016; James and Robson, 2012**). These products are generated by processing images by SfM and MVS algorithms, whose processing task is time-consuming and demanding for a computer, especially in the case of processing by MVS algorithm (**Crawford et al., 2021; Moritani et al., 2020, 2019**).

This paper presents a new data processing method with a novel approach to calculating landslide displacements

from Unmanned Aerial System photogrammetric survey data, based exclusively on SfM algorithm steps without using the MVS algorithm. Therefore, it is faster and computationally simpler than previously used methods.

2. Methods and Materials

In this section, the following is described: (i) the theory behind the new data processing method, (ii) defining the test field with a simulated displacement, and (iii) mission planning and data acquisition.

2.1. The Theory behind the New Data Processing Method

This section explains the theory workflow of the new data processing method through the following steps (see **Figure 1**): (1) image processing, (2) calculating displacements from sparse point clouds, and (3) detecting and removing outliers.

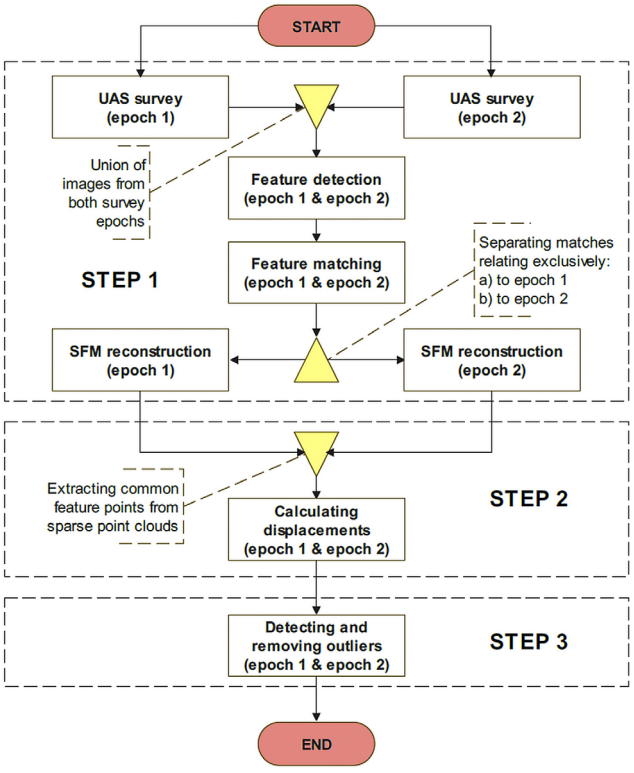

Figure 1: Flowchart of the new data processing method

2.1.1. Image Processing

At the very beginning, the new data processing method starts with the feature detection on all images acquired in two different epochs. The feature on the image represents a distinctive area of an image texture that is likely to be identifiable in other images (**James and Robson, 2012**). Numerous methods can be used for detecting features on images. Some of these methods are the following: Accelerated KAZE Features (AKAZE) (**Alcantarilla et al., 2013**), Speeded Up Robust Features (SURF) (**Bay et al., 2006**), Hessian Affine feature point detector, and Histogram of Oriented Gradients descriptor (HAHOG) (**Meza et al., 2018**), Oriented Fast and Rotated Brief (ORB) (**Rublee et al., 2011**), and Scale Invariant Feature Transform (SIFT) (**Lowe, 2004**) which is the most widely used method in geosciences (**Carrivick et al., 2016**). These methods are implemented in the Open Computer Vision (OpenCV) library (**Kaehler and Bradski, 2017**).

Once features have been detected on all images of both survey epochs, they need to be matched by some feature matching method. The Fast Library for Approximate Nearest Neighbors (FLANN) (**Muja and Lowe, 2009**) matching method is used in this paper, which is also commonly used in photogrammetry (**Fu and Cai, 2016**). One of the key steps of the proposed processing method is to run a feature matching algorithm simultaneously on images from both surveying epochs, which will later enable connecting reconstructed points of two separately processed surveying epochs and determination of the displacement vectors.

The next step of processing is SfM reconstruction, which is used for reconstructing camera positions, external and internal camera calibration parameters, and, most importantly, reconstruction of the scene's geometry (sparse point cloud) (**Fisher et al., 2016; Granshaw, 1980; Snavely et al., 2008; Szeliski, 2011; Triggs et al., 2000; Ullman, 1979**). Reconstruction of the scene using the SfM algorithm is done separately for the first and second surveying epochs.

The results of the reconstruction using the SfM algorithm are sparse point clouds. The sparse point cloud consists of a spatial structure of feature points, whose reconstruction is obtained by the triangulation process based on matches and features, determined in steps of feature detection and feature matching (**Hodlmoser et al., 2013**). Each sparse point cloud represents reconstructed feature points that relate exclusively to the first and exclusively to the second epoch.

Since the SfM algorithm reconstructs the sparse point clouds in local coordinate systems (**Carrivick et al., 2016**), the next step is to associate them with the same global coordinate system by an indirect or direct georeferencing approach. The indirect georeferencing uses a minimum of three Ground Control Points (GCPs) established on the field to calculate a unique seven-parameter linear similarity transformation parameter between the local and global coordinate system (**Carrivick et al., 2016; Oniga et al., 2020**). However, establishing GCPs can sometimes be time-consuming and unfeasible (**Gabrlik et al., 2018**). Moreover, it is beneficial because the GCPs are applied for camera self-calibration in a bundle adjustment to refine the reconstruction (**Bolkas, 2019; Eltner and Schneider, 2015; Jaud et al., 2019**). In contrast to indirect georeferencing, direct georeferencing uses camera position determined with Real-Time Kine-

matic (RTK) or the Post-Processed Kinematic (PPK) GNSS method (**Tsai et al., 2010; Turner et al., 2014; Zhang et al., 2019**). In this case, there is no need to establish the GCPs in the field (**Verhoeven et al., 2012**). Although indirect georeferencing is more time-consuming than direct georeferencing, it is more accurate than direct georeferencing and provides reliable positioning (**Fazeli et al., 2016; Gabrlik et al., 2018; Padró et al., 2019; Zhang et al., 2019**).

2.1.2. Calculating Displacements from Sparse Point Clouds

Considering feature matching is done simultaneously for features in both epochs, numerous reconstructed feature points exist which can be linked together between the two georeferenced sparse point clouds based on the matching results. Displacement vectors are determined by subtracting coordinates of the linked (common) feature points in two surveying epochs:

$$\Delta E_i = E_i(t_2) - E_i(t_1),\ \Delta N_i = N_i(t_2) - N_i(t_1),$$
$$\Delta \mathrm{H}_i = H_i(t_2) - H_i(t_1) \quad (1)$$

Where:

$\Delta E, \Delta N, \Delta H$ – displacement in east, north, and height direction,
i – identification name of the common feature point,
t_1, t_2 – denote the first and second epoch.

2.1.3. Detecting and Removing Outliers

Since the algorithm calculates displacement vectors from all common feature points, it can be assumed that some of them will be outliers that need to be removed from the data. Detecting and removing outliers can be done by performing the Leave-One-Out Cross-Validation (LOOCV) process based on the kriging interpolation (**Mesić Kiš, 2017; Pebesma, 2004; Pebesma and Wesseling, 1998**). That process must be performed separately for displacements in each coordinate direction (ΔE, ΔN, and ΔH), stored in three separate datasets.

Before starting the LOOCV processes, it is possible to filter datasets to make these processes more efficient in terms of the necessary processing power and time. Guided by cognition that the features' reliability increases with the number of images on which they can be found (**Shah et al., 2015; URL 5, 2022**), displacement vectors can be filtered based on the number of images on which each feature point is found.

The most reliable displacements are kept in the datasets by this filtering. Remaining outliers in datasets can be detected and removed by the mentioned LOOCV process based on the kriging interpolation method.

The LOOCV is a cross-validation method where the whole dataset is partitioned into i subsets (S_1 ... S_i), called folds. The number of folds equals the number of observations in the dataset. A validation process is applied i times, for 1 to i, each time using the union of all observations other than S_i as the training set and using S_i observation as the test set (**Sammut and Webb, 2017**). In this paper, the observations are calculated displacements in each coordinate direction.

Detecting and removing outliers starts with calculating parameters for kriging interpolation (semivariogram models) for displacements in each dataset. These parameters are then used to interpolate displacements by the kriging method for each coordinate direction while running the LOOCV processes. In the LOOCV process, the residuals are calculated as a difference between the predicted and observed displacement values. Finally, *z-score* values represent the distance between the predicted and the observed displacement value in standard deviation units, which are calculated separately for each component of the vector (East, North, and Height) as a ratio between the residual and standard deviation of the predicted value:

$$zscore_i = \frac{\widehat{x_i} - x_i}{s_i} \quad (2)$$

Where:

$zscore_i$ – residual divided by standard deviation of the predicted value for each vector component,
$\widehat{x_i}$ – predicted value,
x_i – observed value,
s_i – standard deviation of the predicted value,
i – an index of the data in the datasets.

Guided by the 3-sigma rule, *z-score* values can indicate the presence of outliers in the dataset (**Hawkins, 1980; Jaba, 2007; Kutterer et al., 2003; Lehmann, 2013**). Based on the *z-score (ΔE, ΔN, and ΔH)* values calculated for each displacement in datasets, it is possible to detect outliers among the vectors. Since each displacement vector consists of three displacement components, it is necessary to calculate the *z-score (3D)* value for the whole vector, not just for its components. The *z-score (3D)* value of the displacement vector can be calculated as the square root of the sum of the squared *z-score* values in each coordinate direction:

$$zscore_i(\mathrm{3D}) =$$
$$= \sqrt{zscore_i(\Delta \mathrm{E})^2 + zscore_i(\Delta \mathrm{N})^2 + zscore_i(\Delta \mathrm{H})^2} \quad (3)$$

Where:

$zscore_i$ (3D) – residual divided by standard deviation of the predicted value of the whole vector,
i – an index of the displacement vector.

To apply the 3-sigma rule to the displacement vectors, it is necessary to calculate a threshold, the *max_zscore (3D)* value, above which all vectors with a *z-score (3D)* value greater than that threshold will be considered outliers. The threshold can be calculated as the root of the

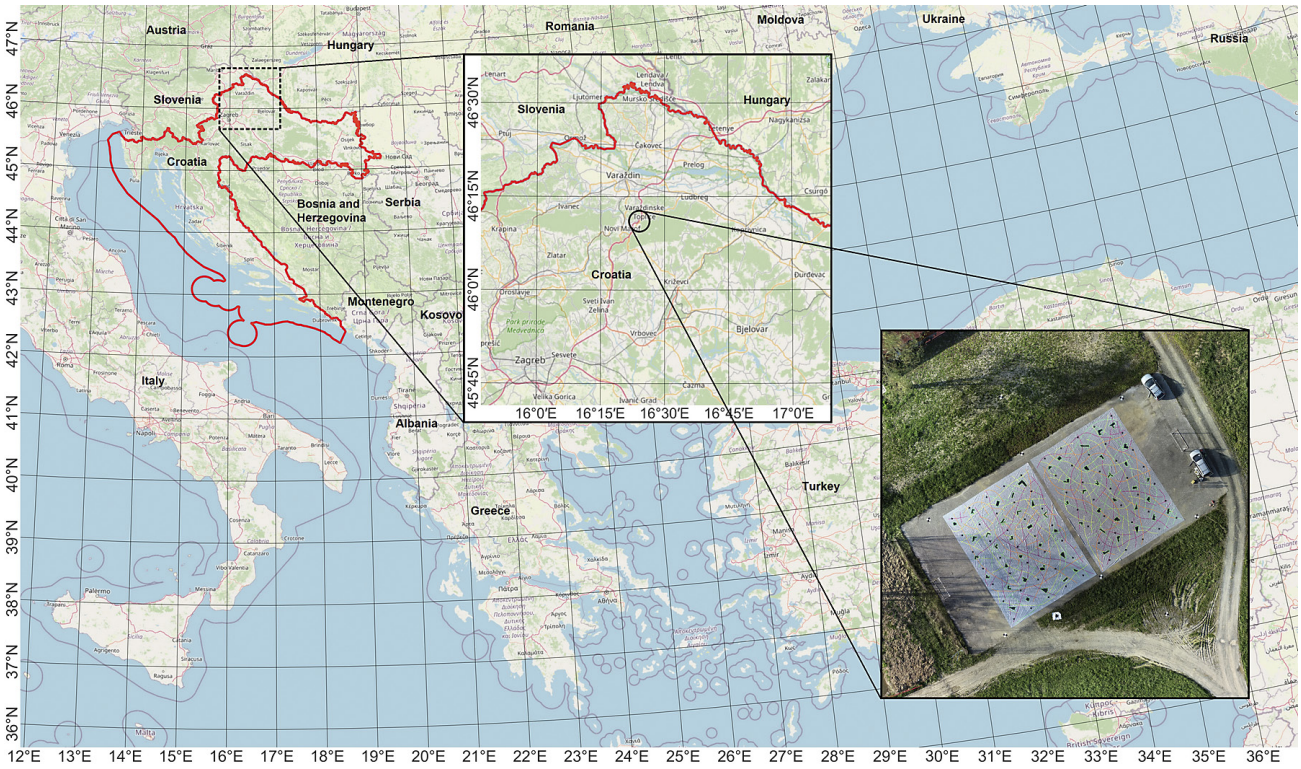

Figure 2: Location of the test field in Croatia (Open Street Map)

sum of the squares of the threshold above which displacement in each separate coordinate direction can be considered as an outlier:

$$max\_zscore(3D) = \\ = \sqrt{\max\_zscore(\Delta E)^2 + \max\_zscore(\Delta N)^2 + max\_zscore(\Delta H)^2} \quad (4)$$

Guided by the 3-sigma rule, the *max_zscore (ΔE, ΔN, and ΔH)* value in each coordinate direction equals 3, which means that the *max_zscore (3D)* value equals 5.2, and any displacement vector with a higher *z-score (3D)* value than *max_zscore (3D)* is considered an outlier.

2.2. Test Field

The UAS photogrammetric surveys were carried out on a test field in the village Kapela Kalnička in the Republic of Croatia (see **Figure 2**). The location coordinates are 46° 11' 3.4" in the north and 16°24' 4.0" in the east, related to the World Geodetic System 84 (WGS 84). The surface of the test field is predominantly horizontal, without significant height differences, mainly covered with grass, and consists of some humans-built artificial objects, such as paths, one house, and a mini football pitch (40 m by 25 m flat concrete surface). A football pitch was used as a test field where landslide movements were simulated. Landslide movements are simulated by moving tarpaulins placed on the top of the pitch. Two large tarpaulins (20 x 15 m) with random patterns and lines drawn to each tarpaulin were used (see **Figure 3**).

The landslide simulation was done by moving tarpaulins in different directions and magnitudes relative to the initial positions. Each tarpaulin was marked with 35 control points (CPs) in the grid of 3 m cell size (see **Figure 4**) to test the accuracy of the new data processing method.

The referent coordinates of the CPs in each epoch were determined with sub-centimeter level accuracy by measurements with the total station. The measurements were done with Leica TPS1201 total station, with an angle measurement accuracy of 1" and a distance measurement accuracy of 2mm+2ppm (**URL 2, 2022**). The reference network used to determine the CPs position in each survey epoch consisted of four points (1P, 2P, 3P, and 4P) stabilized in each corner of the concrete surface. The reference network is of great importance, and therefore steps below explain the process of surveying and determining the coordinates of the reference network points:

1. the initial coordinates of reference network points were determined by GNSS Real-Time-Kinematic (RTK) method using the differential corrections from the CROatian POsitioning System (CROPOS). Each point was measured in two independent measurement repetitions (one repetition consists of 3 consecutive measurements, each lasting 30 seconds) with a time interval of at least 2 hours. The accuracy that can be achieved with this technique is within 2 cm horizontally and within 4 cm vertically (**Bačić et al., 2009; Jakopec et al., 2013; Milec et al., 2015; URL 1, 2022**);

2. the total station was set up by the free-station (resection) method related to the initial coordinates of network points, after which the network points were again measured to determine their final coordinates;

Figure 3: The appearance of the tarpaulins from the ground

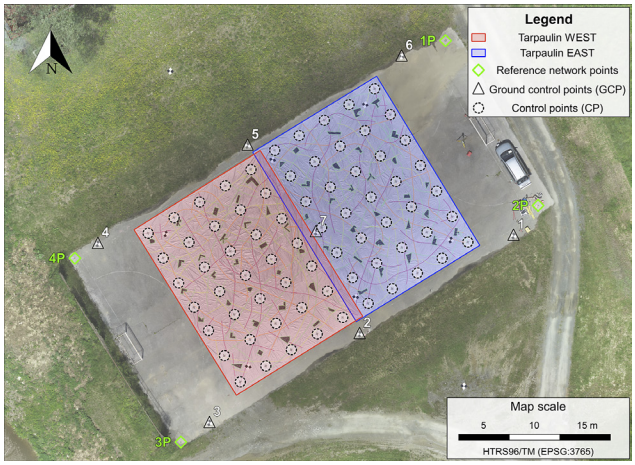

Figure 4: Distribution of the reference network points, CPs, and GCPs on tarpaulins

3. the final coordinates of the network points were used in both survey epochs to set up the total station to determine the true (referent) coordinates of the CPs.

Further, seven GCPs have been established on the test field for UAS indirect georeferencing (see **Figure 4**). The appearance of the GCPs was a flat square plate with 50 cm long sides on which the chessboard pattern was painted in black and white colors (see **Figure 5**). The GCPs coordinates were determined by the GNSS RTK method using the CROPOS, using an identical measurement procedure, as well as when determining the initial coordinates of the network reference points.

2.3. Mission Planning and Data Acquisition

To test the proposed data processing method for determining landslide displacements, it was necessary to conduct a UAS photogrammetric survey. The first step of the UAS photogrammetric survey is to make a flight plan for the UAS mission. Weather forecast is one of the crucial parameters in a UAS mission planning since poor weather conditions (like high and low temperatures, clouds, wind, icing, low visibility, fog, and rain) could potentially postpone the mission (**Kinney et al., 2005; Lindner et al., 2016; Thibbotuwawa et al., 2020**). Only one mission was planned for this research, and it was used in both surveying epochs. The mission was planned and defined in Universal Ground Control Software (UgCS) (**URL 6, 2021**).

The UAS surveys were performed using quadcopter DJI Phantom 4 Pro v2.0, with a built-in 1-inch, 20 Megapixels CMOS camera sensor. The camera lens offers a Field Of View (FOV) of 84° with a focal length range of 8.8 mm/24 mm (35 mm format equivalent) and an aperture of f/2.8 – f/11, with autofocus from 1 m to infinity

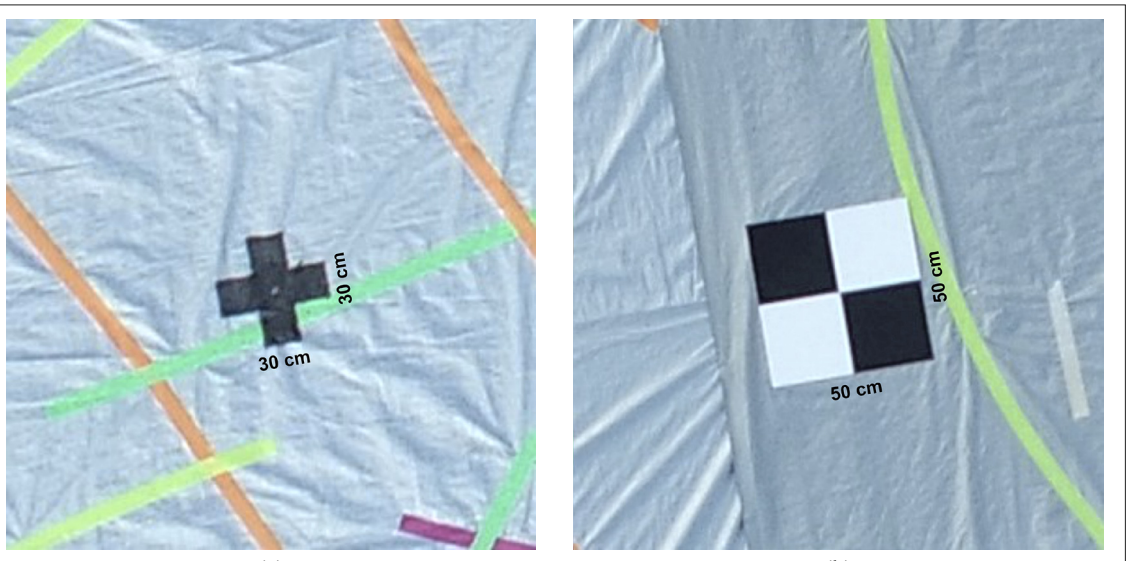

(a) (b)

Figure 5: The appearance of (a) CP marks, and (b) GCP marks

(**URL 4, 2022**). The most significant feature is that the camera has a mechanical shutter that does not cause geometric distortion (**Kuželka and Surový, 2018**).

A double-grid UAS flight (in perpendicular directions) was planned (see **Figure 6**), which is recommended for creating 3D models of the earth's surface (**Röder et al., 2017**). The flight altitude was set at 20 m above ground level, leading to the average ground sample distance (GSD) of 0.60 cm/px. It is good to note that the accuracy of the UAS photogrammetric survey mainly depends on the flight altitude (**Brückl et al., 2006**). Longitudinal overlap was set at 80% and transversely at 85% between images. The camera's tilt was set at 70° (where 0° means that the camera looks horizontal and 90° means that the camera looks straight down). The camera shutter was set to take a photo every 4.23 m. The flight speed was set to 1.40 m/s.

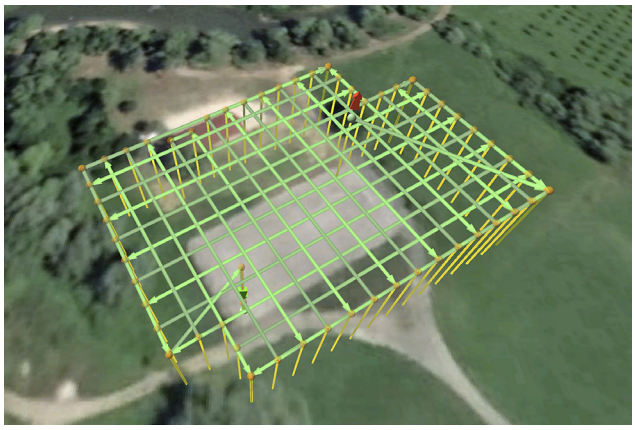

Figure 6: Planned waypoints of UAS mission in software UGCS

This planned mission was surveyed twice, once before and another time after moving tarpaulins, with an interval of 3 hours. The first survey was executed at 1 pm (first survey epoch), and the second flight was executed at 4 pm (second survey epoch). The weather conditions were favorable for a UAS survey. The sky was cloudy with no precipitation, the air temperature was between 12-19°C, and the wind speed was up to 6 m/s with a few gusts. The camera was set on auto mode, which means that parameters were automatically adjusted during the flights. So, the shutter speed ranged from f/5 to f/8, and the aperture ranged from 1/200 to 1/1250). The ISO parameter remained unchanged during the flights and equaled 100. A total of 422 images were acquired in the first survey epoch, and 421 images were acquired in the second survey epoch.

3. Results

This section presents the processing of the collected UAS photogrammetric survey data and analysis of determined displacements. Therefore, it is divided into two subsections for better presentation: (i) application of the new data processing method in practice, and (ii) accuracy of determining landslide displacement by the new data processing method.

3.1. Application and Testing of the New Data Processing Method

Processing UAS images by the new data processing method was done in the software OpenSfM. The OpenSfM is open-source software for geographical alignment and robustness, with the primary purpose of producing a robust and scalable reconstruction model (**URL 3, 2020**). As described in section 2.1.1., the first step in data processing is to detect features on images collected in both surveying epochs. The most common SIFT method was used for feature detection. Approximately 77.8 million features were found on all 843 images, which gives an average of 92.3 thousand features per image.

The next step is to match all these features. The FLANN method was used for the matching process. The results in **Table 1** indicate that 14.7 million matches were found among all image pairs. For this method, matches found between two images are crucial, where one image is from the first, and the other is from the second surveying epoch, so they are called common matches. Over 3 million common matches were detected between the images in both epochs.

A similar number of features were found in the first and second epochs, while more matches were detected between the features on the first epoch images (see **Table 1**).

The total number of all matched feature points (points with features matched between at least two images) found in the first and second epochs counts 1 936 904, whereas 129 153 are common feature points because they are matched between the images of both epochs. The ratio between common and all feature points

Table 1: Total number of features, matches, and matching feature points

	Features	Matches	Matched feature points
All	77 809 980 (100.00%)	14 716 671 (100.00%)	1 936 904 (100.00%)
Epoch 1	37 925 904 (49.00%)	6 805 084 (46.24%)	956 044 (49.36%)
Epoch 2	39 884 076 (51.00%)	4 828 112 (32.81%)	851 707 (43.97%)
Common (Epoch 1 & Epoch 2)		3 083 475 (20.95%)	129 153 (6.67%)
Common (Epoch 1)		2 262 311 (61.30%)*	
Common (Epoch 2)		1 386 846 (38.70%)*	

* The proportion relative to the common matches (Epoch 1 & Epoch 2)

Table 2: The number of all potential matched feature points and the reconstructed feature points

	All potential points	Points founded on only one image	Reconstructed points	
			All	Common
Epoch 1	1 085 197	77 721	888 420	29 423
Epoch 2	980 860	79 707	819 521	

amounts to 6.67%, which means it is possible to determine displacements of approximately every fifteenth feature point.

Comparing the number of common feature points and the number of common matches shows that each feature point is detected on 23 images on average. Determining which proportion of these 23 images is related to a particular epoch shows that 61.30% are related to the first and 38.70% to the second epoch. In other words, on average, each common feature point is detected on approximately 14 images of the first epoch and approximately 9 images of the second epoch.

The discrepancy between the number of features, matches, and matched feature points between the two epochs is most likely because the UAS surveys were performed at different times of the day. The elevation angle of the Sun was lower during the second surveying epoch, leading to greater shadows on the images caused by the obscuring of the sun's light rays by plant vegetation, primarily trees, in the surroundings of the test field.

Further, two SFM reconstructions were performed. The first reconstruction was based on matches and features related exclusively to the images of the first epoch, and the second reconstruction was based on matches and features related exclusively to the images of the second epoch. A total of 1 085 197 potential matched feature points participated in the first reconstruction, out of which 11.90% are common feature points, and the rest are detected exclusively on the images of the first survey epoch. A total of 980 860 potential matched feature points participated in the second reconstruction, out of which 13.17% are common feature points, and the rest are detected exclusively on the images of the second survey epoch.

The final production of SfM reconstructions processes was two sparse point clouds, where one is related to the first, and the second is related to the second survey epoch. Out of all potential feature points which participated in the first reconstruction process, 81.86% (888 420) were finally reconstructed, and in the second reconstruction, 83.55% (819 521) of them were finally reconstructed (see **Table 2**).

The final numbers of reconstructed points in both epochs are fewer than the number of potential candidates because, during the reconstruction process, the geometrically incorrect matches are filtered out by the Random Sample Consensus (RANSAC) method (**Choi et al., 2009; Fischler and Bolles, 1981**). Furthermore, in the matches used in reconstruction processes, some potential feature points have been matched between only one image of the one epoch and one or more images of the other epoch. These feature points cannot be reconstructed in an epoch where they are detected on only one image (**Aliakbarpour et al., 2015**).

Since the sparse point clouds are in local (arbitrary) coordinate systems, they need to be transformed into a global coordinate system, enabling the calculation of displacement vectors between common feature points. This research used indirect georeferencing based on 7 GCPs, whose horizontal coordinates were determined in the Croatian Terrestrial Reference System 1996 in the Transverse Mercator projection (HTRS96/TM), and the height coordinates were determined in the Croatian Reference Height System 1971 (HVRS71). The total number of all reconstructed feature points in both survey epochs equals 1 707 941, and the total number of com-

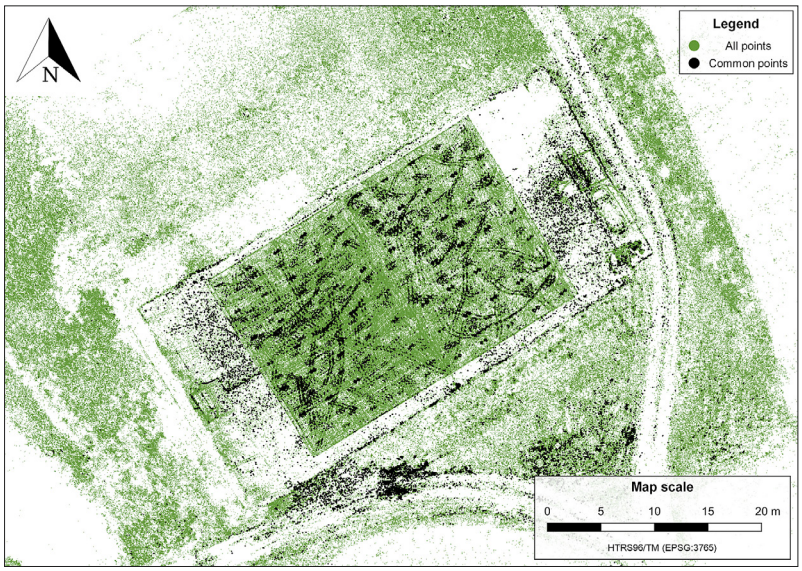

Figure 7: All reconstructed points of both survey epochs and common points between them

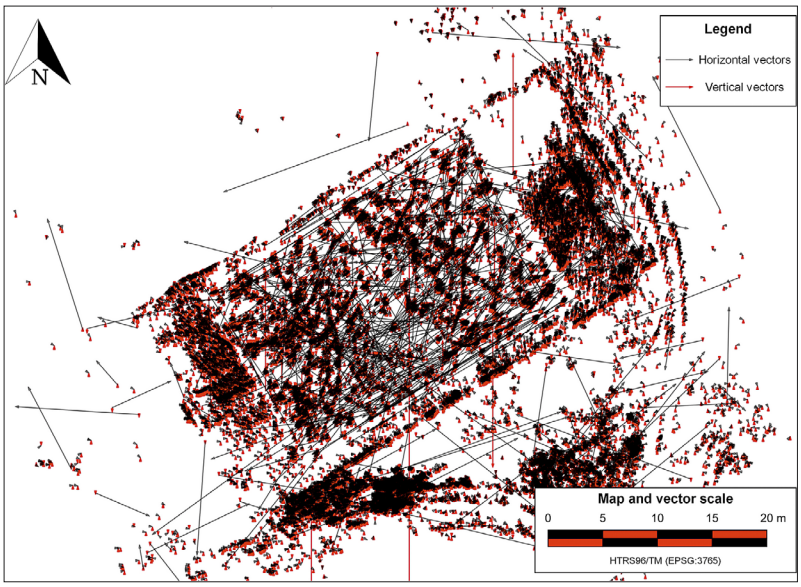

Figure 8: Horizontal and vertical displacement vectors between both survey epochs

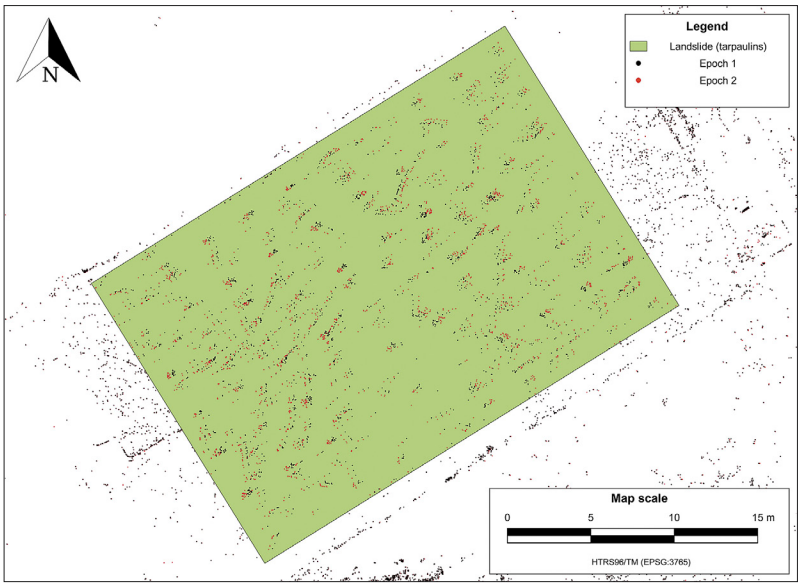

Figure 9: The simulated landslide area and common feature points found on at least five images in both epochs

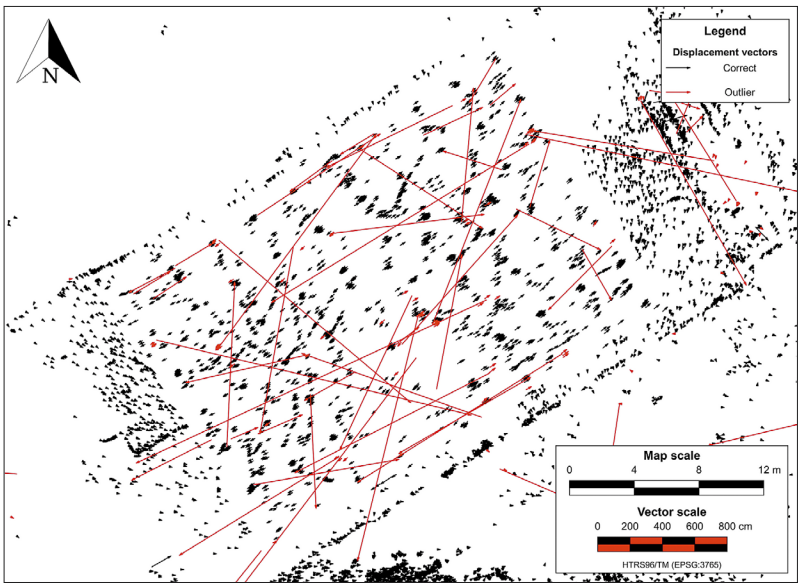

Figure 10: Correct and outlier displacement vectors

Table 3: The statistics of predicted (new data processing method) and referent (total station) displacements vector values for each tarpaulin

Tarpaulin	Statistics values	Predicted displacement			Referent displacement		
		ΔE [cm]	ΔN [cm]	ΔH [cm]	ΔE [cm]	ΔN [cm]	ΔH [cm]
East (n=35)	Min	25.5	19.1	-2.3	25.4	20.4	-0.7
	Max	37.2	29.6	1.8	36.1	29.1	0.4
	Range	11.7	10.5	4.1	10.7	8.7	1.1
	Mean	31.5	23.5	0.0	31.4	24.3	0.0
West (n=35)	Min	-32.5	-25.1	-1.6	-32.5	-24.8	-0.4
	Max	-23.1	-14.3	3.3	-23.5	-13.6	0.4
	Range	9.4	10.8	4.9	9.0	11.2	0.8
	Mean	-27.9	-19.3	0.1	-28.5	-18.7	0.0

Table 4: Statistic of residuals between predicted and referent displacement vectors values.

	Residuals		
	ΔE [cm]	ΔN [cm]	ΔH [cm]
Min	-0.8	-1.9	-2.7
Max	1.9	0.8	3.3
Range	2.7	2.7	6.1
Mean	0.3	-0.7	0.1
St. Dev.	±0.6	±0.5	±0.9

Table 5: RMSE of determining displacements with the new data processing method.

	RMSE		
	ΔE [cm]	ΔN [cm]	ΔH [cm]
1D	±0.6	±0.8	±0.9
2D & 1D	±1.0		±0.9
3D	±1.3		

mon feature points between both survey epochs is 29 423 (see **Table 2**). Their distribution is shown in **Figure 7**.

In the next step, displacements in the east, north, and height direction were calculated as differences between the coordinates of common points. Looking at the distribution of calculated displacement vectors (see **Figure 8**), it can be concluded that numerous displacement vectors differ significantly from others and can be declared as outliers. Hence, we need to remove them from our datasets before any subsequent calculations.

The dataset is filtered before running the outlier removal process, which means that only vectors between feature points found on at least five images in both epochs were kept, by which the number of displacements vector was reduced from 29 423 to 10 213 (see **Figure 9**).

They were further validated to detect and remove outlier displacement vectors from datasets by performing LOOCV processes based on the kriging interpolation method, as explained in section 2.1.3. The total number of removed outlier displacement vectors was 180 (see **Figure 10**). After removing all outliers from datasets, 10033 displacement vectors remained.

3.2. Accuracy of the New Data Processing Method

The landslide displacements determined by the proposed processing method (predicted displacement vectors) were compared with the displacements calculated from total station measurements (referent displacement vectors) to determine the accuracy of the new data processing method. A comparison was made for all 70 CPs (i.e. 35 per tarpaulin). The referent values of the displacements were defined as coordinate differences between the CPs in the first and second survey epoch. The predicted displacement vectors at the CPs were determined by applying the kriging interpolation method.

The predicted vectors indicate that the average movement of the east tarpaulin was 39.3 cm in the northeast direction (53°), and for the west tarpaulin, it was 33.9 cm in the southwest direction (235°). Regarding reference values, they indicate that the average movement of the east tarpaulin was 39.7 cm in the northeast (52°), and for the west tarpaulin, it was 34.1 cm in the southwest direction (237°). By comparing these results, we can notice that the predicted and referent vector values are nearly identical because average vector magnitudes did not differ more than 0.4 cm and more than 2° in any direction (see **Table 3**). Further, the average values of the vertical displacements were equal to zero, which was expected since tarpaulins were moved along the flat horizontal area. The range between displacements for each coordinate direction is not equal to zero, indicating that tarpaulins were not moved evenly along the entire surface.

Displacement residuals are calculated as a difference between referent and displacement values determined by the proposed method (see **Table 4**). The residuals in the horizontal direction range between -1.9 cm to 1.9 cm, and in the vertical direction are between -2.7 cm and 3.3 cm. The mean values of residuals in the east direction are 0.3 cm, -0.7 cm in the north direction, and 0.1 cm in the vertical direction. The standard deviation in

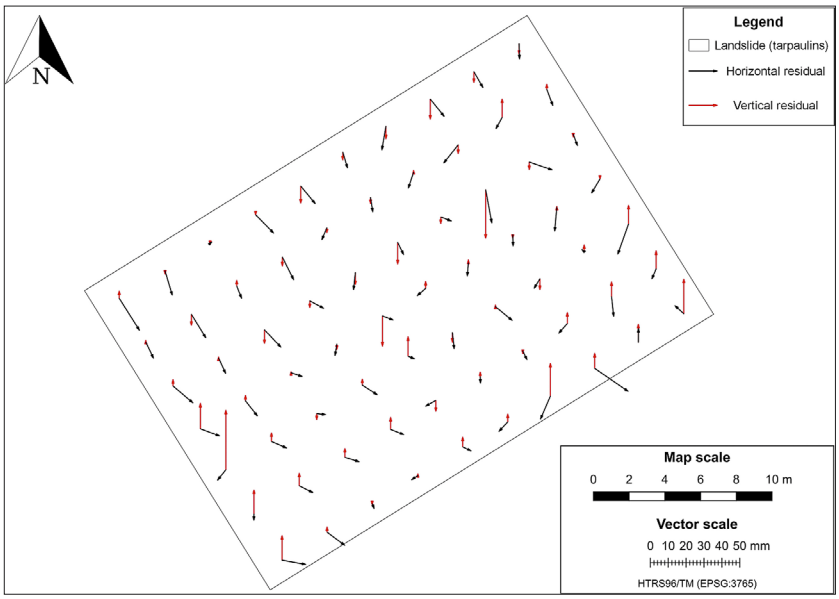

Figure 11: Horizontal and vertical residuals of the new data processing method

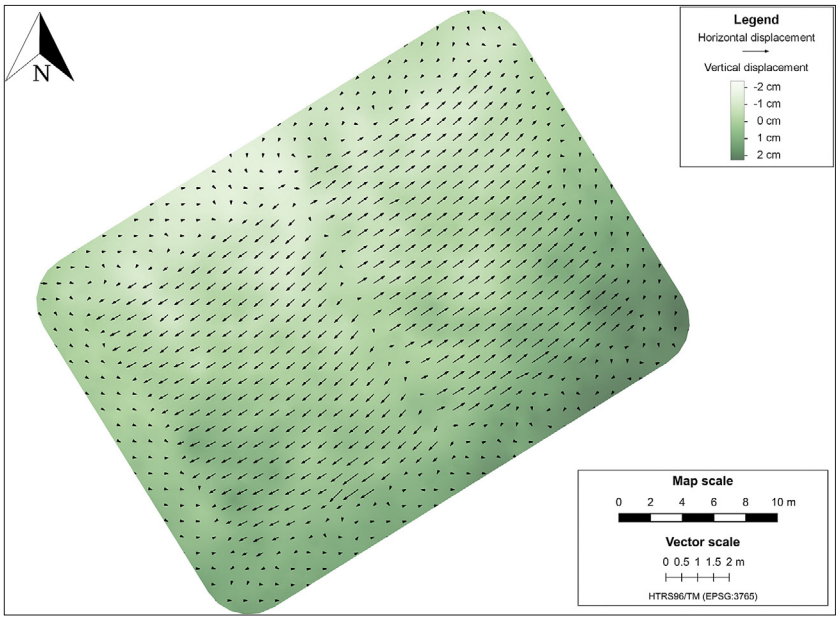

Figure 12: Landslide map with horizontal and vertical displacements

the east direction is ±0.6 cm, in the north direction is ±0.5 cm, and in the vertical direction, it is ±0.6 cm. The results indicate that the displacements are determined with a centimeter-level precision in both horizontal and vertical directions. The graphical presentation of the displacement residuals is shown in **Figure 11**.

Root Mean Square Error (RMSE) of determining displacements is used to measure achieved accuracy (see **Table 5**).

A comparison of the precision and accuracy (St. Dev vs. RMSE) indicates that displacements determined by the new method are not influenced by any systematic errors, which can be confirmed by looking at **Figure 11**. The graphical presentation of determined horizontal and vertical displacements is shown in **Figure 12**.

4. Discussion

The ability to determine displacements from UAS photogrammetric survey using the suggested novel processing method is presented in the previous section. The presented test case shows that displacements with a magnitude of 20 cm can be determined without any issues. Further, accuracy analysis of determining displacements showed the potential of detecting displacements with a magnitude of only a few centimeters since RMSE values were approximately 1 cm.

However, it is important to note that the flight altitude in this research was 20 m above the ground, and the test field area was relatively small compared to an actual landslide. It is questionable what the results would be if

there were higher altitudes and a larger area. Furthermore, the tarpaulins were moved on a flat football pitch, which led to no height differences between epochs. Therefore, future work should investigate how higher flight altitudes over a larger area with diverse topography will affect the accuracy of the new data processing method.

The UAS surveys performed at different times of day will have a difference in light direction and shadows. Having different shadows in two measurement epochs will impact feature detection and feature matching, affecting the accuracy of determining displacements. This was not considered in this paper since tarpaulins were placed on a flat terrain, and therefore, there were no shadows on the collected images. Nevertheless, the influence of the different shadows between different epochs could be investigated by adding three-dimensional features on top of the tarpaulins.

Many factors influenced the achieved accuracy. The most influential is the UAS flight altitude because it significantly affects the GSD value along with the used camera for capturing images. In other words, the lower the flight altitude, the lower the GSD value will be, which will lead to the possibility of detecting very small magnitudes of landslide displacement with great accuracy. Moreover, future work will be related to additional testing of the new data processing method with images acquired from different UAS flight altitudes since the UAS flight altitude significantly dictates the GSD value on acquired images, and thus the accuracy of determining displacement.

Accuracy is also affected by the positioning accuracy of the GCPs. Therefore, they must be well signalized and accurately determined on the field. In other words, the GCPs must be well visible and recognizable in the acquired images, which will lead to accurate georeferenced and refined sparse point clouds.

Since the GSD value is affected by the change in the distance between the camera and the observed object, it is desirable during UAS mission planning to set the vehicle to fly relatively above the ground, which would lead to the GSD value being as stable as possible during UAS measurements on each acquired image.

Also, using the appropriate vehicle and camera for the given task is essential. Choosing proper vehicle flight altitude, speed, and image overlap is important. When choosing a suitable camera and its parameters, the most important indicators are the quality of camera lenses and their distortion, sensor type and size, and shutter type. The most crucial steps of the suggested method are feature detecting and feature matching. Improvements in these steps could produce more matched points between two surveying epochs, potentially increasing the accuracy and reliability of determining displacements. In this paper, features were detected using the SIFT method and matched using the FLANN method. Potentially, one could use different methods or combine multiple methods to get better results. Thus, future work could test several types of feature detection and feature matching methods in processing images with the algorithm of the new method to decide which of them can give the most accurate results.

This paper presented the feasibility of the suggested method in ideal conditions on a relatively small test field. In future work, it is necessary to show the applicability of the suggested method for determining displacements of actual landslides, where the surface consists of diverse, complex topography. This will significantly complicate the possibility of detecting and matching feature points on images of a landslide. The Kostanjek Landslide can serve this purpose since it already has an established continuous real-time monitoring system.

Furthermore, in future work, the new method should be compared with existing methods where the determination of displacement is based on comparisons of dense point clouds, digital terrain models, and digital orthomosaics, whose production is based on processing UAS images with the SfM-MVS algorithm.

5. Conclusions

Landslides represent great danger that can cause fatalities and huge property damage. Understanding the behaviour of landslides and identifying their possible triggering effects usually requires a good knowledge of the kinematics surface and subsurface sliding masses.

Geodetic surveying techniques can be used for landslide monitoring and creating a kinematic model of the landslide. The monitoring technique based on the Unmanned Aerial Systems (UAS) photogrammetric survey is increasingly used for landslide monitoring. This article presents a novel approach to processing UAS photogrammetric survey data for landslide monitoring.

The proposed method relies on matching features between images acquired in two different survey epochs, which enables the calculation of the displacements between the points of the two sparse point clouds. Therefore, there is no need to produce dense point clouds, digital terrain models, or orthomosaic maps, making it faster than previous methods.

The UAS photogrammetric surveys were performed on the test field with simulated displacements to demonstrate the method's applicability. The simulated displacements ranged between 20 and 40 cm and were simulated in an area of approximately 600 square meters. These simulated displacements were determined using the new data processing method and compared to the actual values determined by total station measurements. In the defined test field, the horizontal displacements were determined with an accuracy of ±1.0 cm, and the vertical displacements were determined with an accuracy of ±0.9 cm. These results indicate that the 3D displacements have been determined with an accuracy

of ±1.3 cm. These results were obtained based on the processing of images collected from a height of 20 meters above the ground, which is essential to emphasize because UAS flight altitude plays one of the essential roles in defining the final accuracy of displacement vector determination.

Finally, it can be concluded that the proposed data processing method can successfully and accurately determine landslide displacements, which allows for the detailed definition of landslide surfaces.

6. References

Abellán, A., Calvet, J., Vilaplana, J.M., Blanchard, J. (2010): Detection and spatial prediction of rockfalls by means of terrestrial laser scanner monitoring. Geomorphology, 119, 162–171. https://doi.org/10.1016/j.geomorph.2010.03.016

Abellán, A., Jaboyedoff, M., Oppikofer, T., Vilaplana, J.M. (2009): Detection of millimetric deformation using a terrestrial laser scanner: experiment and application to a rockfall event. Natural Hazards and Earth System Sciences, 9, 365–372. https://doi.org/10.5194/nhess-9-365-2009

Acar, M., Ozludemir, M.T., Erol, S., Celik, R.N., Ayan, T. (2008): Kinematic landslide monitoring with Kalman filtering. Natural Hazards and Earth System Science, 8, 213–221. https://doi.org/10.5194/nhess-8-213-2008

Adriano, B., Yokoya, N., Miura, H., Matsuoka, M., Koshimura, S. (2020): A Semiautomatic Pixel-Object Method for Detecting Landslides Using Multitemporal ALOS-2 Intensity Images. Remote Sensing, 12, 561. https://doi.org/10.3390/rs12030561

Afeni, T.B., Cawood, F.T. (2013): Slope Monitoring using Total Station: What are the Challenges and How Should These be Mitigated? South African Journal of Geomatics, 2, 41–53.

Ai, M., Hu, Q., Li, J., Wang, M., Yuan, H., Wang, S. (2015): A Robust Photogrammetric Processing Method of Low-Altitude UAV Images. Remote Sensing, 7, 2302–2333. https://doi.org/10.3390/rs70302302

Aimaiti, Y., Liu, W., Yamazaki, F., Maruyama, Y. (2019): Earthquake-Induced Landslide Mapping for the 2018 Hokkaido Eastern Iburi Earthquake Using PALSAR-2 Data. Remote Sensing, 11, 2351. https://doi.org/10.3390/rs11202351

Alcantarilla, P., Nuevo, J., Bartoli, A. (2013): Fast Explicit Diffusion for Accelerated Features in Nonlinear Scale Spaces, in: Procedings of the British Machine Vision Conference 2013. British Machine Vision Association, pp. 13.1-13.11. https://doi.org/10.5244/C.27.13

Aliakbarpour, H., Palaniappan, K., Seetharaman, G. (2015): Robust Camera Pose Refinement and Rapid SfM for Multiview Aerial Imagery—Without RANSAC. IEEE Geoscience and Remote Sensing Letters, 12, 2203–2207. https://doi.org/10.1109/LGRS.2015.2457299

Anders, K., Winiwarter, L., Lindenbergh, R., Williams, J.G., Vos, S.E., Höfle, B. (2020): 4D objects-by-change: Spatiotemporal segmentation of geomorphic surface change from LiDAR time series. ISPRS Journal of Photogrammetry and Remote Sensing, 159, 352–363. https://doi.org/10.1016/j.isprsjprs.2019.11.025

Arbanas, S., Arbanas, Ž., Bernat, S., Krkač, M., Kalinić, P., Martinović, K., Sajko, J., Fabris, N., Antolović, A. (2013): Upravljanje kriznim situacijama uslijed pokretanja klizišta (*Management of the crisis situations caused by landslide activations*). V. Konferencija Hrvatske platforme za smanjenje rizika od katastrofa. (*in Croatian*)

Ardizzone, F., Cardinali, M., Galli, M., Guzzetti, F., Reichenbach, P. (2007): Identification and mapping of recent rainfall-induced landslides using elevation data collected by airborne Lidar. Natural Hazards and Earth System Sciences, 7, 637–650. https://doi.org/10.5194/nhess-7-637-2007

Artese, S., Perrelli, M. (2018): Monitoring a Landslide with High Accuracy by Total Station: A DTM-Based Model to Correct for the Atmospheric Effects. Geosciences, 8, 46. https://doi.org/10.3390/geosciences8020046

Bačić, Ž., Marjanović, M., Bosiljevac, M. (2009): CROPOS – Croatian Positioning System CROPOS, in: FIG Working Week 2009 – Surveyors Key Role in Accelerated Development.

Baltsavias, E.P. (1999): A comparison between photogrammetry and laser scanning. ISPRS Journal of Photogrammetry and Remote Sensing, 54, 83–94. https://doi.org/10.1016/S0924-2716(99)00014-3

Barbarella, M., Fiani, M. (2013): Monitoring of large landslides by Terrestrial Laser Scanning techniques: field data collection and processing. European Journal of Remote Sensing, 46, 126–151. https://doi.org/10.5721/EuJRS20134608

Bardi, F., Raspini, F., Frodella, W., Lombardi, L., Nocentini, M., Gigli, G., Morelli, S., Corsini, A., Casagli, N. (2017): Monitoring the Rapid-Moving Reactivation of Earth Flows by Means of GB-InSAR: The April 2013 Capriglio Landslide (Northern Appennines, Italy). Remote Sensing, 9, 165. https://doi.org/10.3390/rs9020165

Barnhart, T., Crosby, B. (2013): Comparing Two Methods of Surface Change Detection on an Evolving Thermokarst Using High-Temporal-Frequency Terrestrial Laser Scanning, Selawik River, Alaska. Remote Sensing, 5, 2813–2837. https://doi.org/10.3390/rs5062813

Bay, H., Tuytelaars, T., Van Gool, L. (2006): SURF: Speeded Up Robust Features, in: Lecture Notes in Computer Science (Including Subseries Lecture Notes in Artificial Intelligence and Lecture Notes in Bioinformatics). pp. 404–417. https://doi.org/10.1007/11744023_32

Benjamin, J., Rosser, N., Brain, M. (2016): Rockfall detection and volumetric characterisation using LiDAR, in: Landslides and Engineered Slopes. Experience, Theory and Practice. CRC Press, pp. 389–395. https://doi.org/10.1201/b21520-38

Bolkas, D. (2019): Assessment of GCP Number and Separation Distance for Small UAS Surveys with and without GNSS-PPK Positioning. Journal of Surveying Engineering, 145, 04019007. https://doi.org/10.1061/(ASCE)SU.1943-5428.0000283

Bonneau, D.A., Hutchinson, D.J. (2019): The use of terrestrial laser scanning for the characterization of a cliff-talus system in the Thompson River Valley, British Columbia,

Canada. Geomorphology, 327, 598–609. https://doi.org/10.1016/j.geomorph.2018.11.022

Bozzano, F., Mazzanti, P., Perissin, D., Rocca, A., De Pari, P., Discenza, M. (2017): Basin Scale Assessment of Landslides Geomorphological Setting by Advanced InSAR Analysis. Remote Sensing, 9, 267. https://doi.org/10.3390/rs9030267

Brückl, E., Brunner, F.K., Kraus, K. (2006): Kinematics of a deep-seated landslide derived from photogrammetric, GPS and geophysical data. Engineering Geology, 88, 149–159. https://doi.org/10.1016/j.enggeo.2006.09.004

Burrows, K., Walters, R.J., Milledge, D., Spaans, K., Densmore, A.L. (2019): A New Method for Large-Scale Landslide Classification from Satellite Radar. Remote Sensing, 11, 237. https://doi.org/10.3390/rs11030237

Carrivick, J.L., Smith, M.W., Quincey, D.J. (2016): Structure from Motion in the Geosciences. John Wiley & Sons, Ltd, Chichester, UK. https://doi.org/10.1002/9781118895818

Castagnetti, C., Bertacchini, E., Corsini, A., Rivola, R. (2014): A reliable methodology for monitoring unstable slopes: the multi-platform and multi-sensor approach, in: Michel, U., Schulz, K. (Eds.), Earth Resources and Environmental Remote Sensing/GIS Applications V. p. 92450J. https://doi.org/10.1117/12.2067407

Choi, S., Kim, T., Yu, W. (2009): Performance Evaluation of RANSAC Family, in: Procedings of the British Machine Vision Conference 2009. British Machine Vision Association, pp. 81.1-81.12. https://doi.org/10.5244/C.23.81

Clapuyt, F., Vanacker, V., Schlunegger, F., Van Oost, K. (2017): Unravelling earth flow dynamics with 3-D time series derived from UAV-SfM models. Earth Surface Dynamics, 5, 791–806. https://doi.org/10.5194/esurf-5-791-2017

Cook, K.L. (2017): An evaluation of the effectiveness of low-cost UAVs and structure from motion for geomorphic change detection. Geomorphology, 278, 195–208. https://doi.org/10.1016/j.geomorph.2016.11.009

Crawford, B., Swanson, E., Schultz-Fellenz, E., Collins, A., Dann, J., Lathrop, E., Milazzo, D. (2021): A New Method for High Resolution Surface Change Detection: Data Collection and Validation of Measurements from UAS at the Nevada National Security Site, Nevada, USA. Drones, 5, 25. https://doi.org/10.3390/drones5020025

Cruden, D.M. (1991): A simple definition of a landslide. Bulletin of the International Association of Engineering Geology -Bulletin de l'Association Internationale de Géologie de l'Ingénieur, 43, 27–29. https://doi.org/10.1007/BF02590167

DiFrancesco, P.-M., Bonneau, D., Hutchinson, D.J. (2020): The Implications of M3C2 Projection Diameter on 3D Semi-Automated Rockfall Extraction from Sequential Terrestrial Laser Scanning Point Clouds. Remote Sensing, 12, 1885. https://doi.org/10.3390/rs12111885

Du, Y., Xu, Q., Zhang, L., Feng, G., Li, Z., Chen, R.-F., Lin, C.-W. (2017): Recent Landslide Movement in Tsaoling, Taiwan Tracked by TerraSAR-X/TanDEM-X DEM Time Series. Remote Sensing, 9, 353. https://doi.org/10.3390/rs9040353

Eeckhaut, M. Van Den, Poesen, J., Verstraeten, G., Vanacker, V., Nyssen, J., Moeyersons, J., Beek, L.P.H. van, Vandekerckhove, L. (2007): Use of LIDAR-derived images for mapping old landslides under forest. Earth Surface Processes and Landforms, 32, 754–769. https://doi.org/10.1002/esp.1417

Eker, R., Aydın, A., Hübl, J. (2018): Unmanned aerial vehicle (UAV)-based monitoring of a landslide: Gallenzerkogel landslide (Ybbs-Lower Austria) case study. Environmental Monitoring and Assessment, 190, 28. https://doi.org/10.1007/s10661-017-6402-8

Eltner, A., Kaiser, A., Castillo, C., Rock, G., Neugirg, F., Abellán, A. (2016): Image-based surface reconstruction in geomorphometry – merits, limits and developments. Earth Surface Dynamics, 4, 359–389. https://doi.org/10.5194/esurf-4-359-2016

Eltner, A., Schneider, D. (2015): Analysis of Different Methods for 3D Reconstruction of Natural Surfaces from Parallel-Axes UAV Images. The Photogrammetric Record, 30, 279–299. https://doi.org/10.1111/phor.12115

Esposito, G., Mastrorocco, G., Salvini, R., Oliveti, M., Starita, P. (2017a): Application of UAV photogrammetry for the multi-temporal estimation of surface extent and volumetric excavation in the Sa Pigada Bianca open-pit mine, Sardinia, Italy. Environmental Earth Sciences, 76, 103. https://doi.org/10.1007/s12665-017-6409-z

Esposito, G., Salvini, R., Matano, F., Sacchi, M., Danzi, M., Somma, R., Troise, C. (2017b): Multitemporal monitoring of a coastal landslide through SfM-derived point cloud comparison. The Photogrammetric Record, 32, 459–479. https://doi.org/10.1111/phor.12218

Fazeli, H., Samadzadegan, F., Dadrasjavan, F. (2016): Evaluating the potential of RTK-UAV for automatic point cloud generation in 3D rapid mapping. ISPRS – International Archives of the Photogrammetry, Remote Sensing and Spatial Information Sciences, XLI-B6, 221–226. https://doi.org/10.5194/isprsarchives-XLI-B6-221-2016

Fernández, T., Pérez, J., Cardenal, J., Gómez, J., Colomo, C., Delgado, J. (2016): Analysis of Landslide Evolution Affecting Olive Groves Using UAV and Photogrammetric Techniques. Remote Sensing, 8, 837. https://doi.org/10.3390/rs8100837

Fiorucci, F., Cardinali, M., Carlà, R., Rossi, M., Mondini, A.C., Santurri, L., Ardizzone, F., Guzzetti, F. (2011): Seasonal landslide mapping and estimation of landslide mobilization rates using aerial and satellite images. Geomorphology, 129, 59–70. https://doi.org/10.1016/j.geomorph.2011.01.013

Fischler, M.A., Bolles, R.C. (1981): Random sample consensus: A Paradigm for Model Fitting with Applications to Image Analysis and Automated Cartography. Communications of the ACM, 24, 381–395. https://doi.org/10.1145/358669.358692

Fisher, R.B., Breckon, T.P., Dawson-Howe, K., Fitzgibbon, A., Robertson, C., Trucco, E., Williams, C.K.I. (2016): Dictionary of Computer Vision and Image Processing, 2nd ed, Journal of Electronic Imaging. John Wiley & Sons, Ltd, Chichester, UK. https://doi.org/10.1002/9781119286462

Fraser, C.S., Cronk, S. (2009): A hybrid measurement approach for close-range photogrammetry. ISPRS Journal of

Photogrammetry and Remote Sensing, 64, 328–333. https://doi.org/10.1016/j.isprsjprs.2008.09.009

Fu, C., Cai, D. (2016): EFANNA : An Extremely Fast Approximate Nearest Neighbor Search Algorithm Based on kNN Graph.

Gabrlik, P., Cour-Harbo, A. la, Kalvodova, P., Zalud, L., Janata, P. (2018): Calibration and Accuracy Assessment in a Direct Georeferencing System for UAS Photogrammetry. International Journal of Remote Sensing, 39, 4931–4959. https://doi.org/10.1080/01431161.2018.1434331

Galli, M., Ardizzone, F., Cardinali, M., Guzzetti, F., Reichenbach, P. (2008): Comparing landslide inventory maps. Geomorphology, 94, 268–289. https://doi.org/10.1016/j.geomorph.2006.09.023

Ge, Gokon, Meguro, Koshimura (2019): Study on the Intensity and Coherence Information of High-Resolution ALOS-2 SAR Images for Rapid Massive Landslide Mapping at a Pixel Level. Remote Sensing, 11, 2808. https://doi.org/10.3390/rs11232808

Granshaw, S.I. (1980): Bundle adjustment methods in engineering photogrammetry. The Photogrammetric Record, 10, 181–207. https://doi.org/10.1111/j.1477-9730.1980.tb00020.x

Hawkins, D.M. (1980): Identification of Outliers, Identification of Outliers. Springer Netherlands, Dordrecht. https://doi.org/10.1007/978-94-015-3994-4

Hodlmoser, M., Micusik, B., Kampel, M. (2013): Sparse Point Cloud Densification by Combining Multiple Segmentation Methods, in: 2013 International Conference on 3D Vision. IEEE, pp. 438–445. https://doi.org/10.1109/3DV.2013.64

Hsieh, Y.-C., Chan, Y.-C., Hu, J.-C. (2016): Digital Elevation Model Differencing and Error Estimation from Multiple Sources: A Case Study from the Meiyuan Shan Landslide in Taiwan. Remote Sensing, 8, 199. https://doi.org/10.3390/rs8030199

Huang, H., Long, J., Lin, H., Zhang, L., Yi, W., Lei, B. (2017): Unmanned aerial vehicle based remote sensing method for monitoring a steep mountainous slope in the Three Gorges Reservoir, China. Earth Science Informatics, 10, 287–301. https://doi.org/10.1007/s12145-017-0291-9

Jaba, E. (2007): The "3 sigma" rule used for the identification of the regional disparities. The yearbook of the "Gh. Zane" Institute of Economic Research, 16, 47–56.

Jaboyedoff, M., Choffet, M., Derron, M.-H., Horton, P., Loye, A., Longchamp, C., Mazotti, B., Michoud, C., Pedrazzini, A. (2012): Preliminary Slope Mass Movement Susceptibility Mapping Using DEM and LiDAR DEM, in: Terrigenous Mass Movements. Springer Berlin Heidelberg, Berlin, Heidelberg, pp. 109–170. https://doi.org/10.1007/978-3-642-25495-6_5

Jaboyedoff, M., Demers, D., Locat, J., Locat, A., Locat, P., Oppikofer, T., Robitaille, D., Turmel, D. (2009): Use of terrestrial laser scanning for the characterization of retrogressive landslides in sensitive clay and rotational landslides in river banks. Canadian Geotechnical Journal, 46, 1379–1390. https://doi.org/10.1139/T09-073

Jakopec, I., Marendić, A., Paar, R., Grgac, I., Tomić, H., Krkač, M., Letunić, T. (2021): Periodic Monitoring of the Kostanjek Landslide Using UAV, in: Springer Proceedings in Earth and Environmental Sciences. pp. 236–245. https://doi.org/10.1007/978-3-030-51953-7_20

Jakopec, I., Šugar, D., Bačić, Ž. (2013): Ispitivanje točnosti VPPS usluge CROPOS-a (*Testing accuracy of CROPOS VPPS service*), in: 3. CROPOS Konferencija. pp. 141–149. (*in Croatian*)

James, M.R., Robson, S. (2014): Mitigating systematic error in topographic models derived from UAV and ground-based image networks. Earth Surface Processes and Landforms, 39, 1413–1420. https://doi.org/10.1002/esp.3609

James, M.R., Robson, S. (2012): Straightforward reconstruction of 3D surfaces and topography with a camera: Accuracy and geoscience application. Journal of Geophysical Research: Earth Surface, 117. https://doi.org/10.1029/2011JF002289

James, M.R., Robson, S., D'Oleire-Oltmanns, S., Niethammer, U. (2017): Optimising UAV topographic surveys processed with structure-from-motion: Ground control quality, quantity and bundle adjustment. Geomorphology, 280, 51–66. https://doi.org/10.1016/j.geomorph.2016.11.021

Jaud, M., Passot, S., Allemand, P., Le Dantec, N., Grandjean, P., Delacourt, C. (2019): Suggestions to Limit Geometric Distortions in the Reconstruction of Linear Coastal Landforms by SfM Photogrammetry with PhotoScan® and MicMac® for UAV Surveys with Restricted GCPs Pattern. Drones, 3. https://doi.org/10.3390/drones3010002

Kaehler, A., Bradski, G. (2017): Learning OpenCV 3: Computer vision in C++ with the OpenCV library.

Kang, Y., Zhao, C., Zhang, Q., Lu, Z., Li, B. (2017): Application of InSAR Techniques to an Analysis of the Guanling Landslide. Remote Sensing, 9, 1046. https://doi.org/10.3390/rs9101046

Kasperski, J., Delacourt, C., Allemand, P., Potherat, P., Jaud, M., Varrel, E. (2010): Application of a Terrestrial Laser Scanner (TLS) to the Study of the Séchilienne Landslide (Isère, France). Remote Sensing, 2, 2785–2802. https://doi.org/10.3390/rs122785

Kinney, G.W., Hill, R.R., Moore, J.T. (2005): Devising a quick-running heuristic for an unmanned aerial vehicle (UAV) routing system. Journal of the Operational Research Society, 56, 776–786. https://doi.org/10.1057/palgrave.jors.2601867

Krkač, M., Bernat Gazibara, S., Sečanj, M., Arbanas, Ž., Mihalić Arbanas, S. (2019): Continuous monitoring of the Kostanjek landslide, in: Proceedings of the 4th Regional Symposium on Landslides in the Adriatic – Balkan Region. Društvo za geotehniku u Bosni i Hercegovini, pp. 43–48. https://doi.org/10.35123/ReSyLAB_2019_7

Krkač, M., Bernat Gazibara, S., Sečanj, M., Sinčić, M., Mihalić Arbanas, S. (2021): Kinematic model of the slow-moving Kostanjek landslide in Zagreb, Croatia. Rudarsko-Geolosko-Naftni Zbornik, 36, 59–68. https://doi.org/10.17794/rgn.2021.2.6

Kromer, R., Abellán, A., Hutchinson, D., Lato, M., Edwards, T., Jaboyedoff, M. (2015): A 4D Filtering and Calibration Technique for Small-Scale Point Cloud Change Detection with a Terrestrial Laser Scanner. Remote Sensing, 7, 13029–13052. https://doi.org/10.3390/rs71013029

Kromer, R.A., Abellán, A., Hutchinson, D.J., Lato, M., Chanut, M.A., Dubois, L., Jaboyedoff, M. (2017): Automated terrestrial laser scanning with near-real-time change detection – Monitoring of the Séchilienne landslide. Earth Surface Dynamics, 5, 293–310. https://doi.org/10.5194/esurf-5-293-2017

Kutterer, H., Heinkelmann, R., Tesmer, V. (2003): Robust Outlier Detection in VLBI Data Analysis, in: Proceedings of the 16th Working Meeting on European VLBI for Geidesy and Astrometry. Leipzig/Frankfurt, pp. 247–256.

Kuželka, K., Surový, P. (2018): Mapping Forest Structure Using UAS inside Flight Capabilities. Sensors, 18, 2245. https://doi.org/10.3390/s18072245

Lague, D., Brodu, N., Leroux, J. (2013): Accurate 3D comparison of complex topography with terrestrial laser scanner: Application to the Rangitikei canyon (N-Z). ISPRS Journal of Photogrammetry and Remote Sensing, 82, 10–26. https://doi.org/10.1016/j.isprsjprs.2013.04.009

Lehmann, R. (2013): 3σ-Rule for Outlier Detection from the Viewpoint of Geodetic Adjustment. Journal of Surveying Engineering, 139, 157–165. https://doi.org/10.1061/(ASCE)SU.1943-5428.0000112

Leprince, S., Barbot, S., Ayoub, F., Avouac, J.-P. (2007): Automatic and Precise Orthorectification, Coregistration, and Subpixel Correlation of Satellite Images, Application to Ground Deformation Measurements. IEEE Transactions on Geoscience and Remote Sensing, 45, 1529–1558. https://doi.org/10.1109/TGRS.2006.888937

Lin, J., Tao, H., Wang, Y., Huang, Z. (2010): Practical application of unmanned aerial vehicles for mountain hazards survey, in: 2010 18th International Conference on Geoinformatics. IEEE, pp. 1–5. https://doi.org/10.1109/GEOINFORMATICS.2010.5567777

Lindner, G., Schraml, K., Mansberger, R., Hübl, J. (2016): UAV monitoring and documentation of a large landslide. Applied Geomatics, 8, 1–11. https://doi.org/10.1007/s12518-015-0165-0

Lowe, D.G. (2004): Distinctive Image Features from Scale-Invariant Keypoints. International Journal of Computer Vision, 60, 91–110. https://doi.org/10.1023/B:VISI.0000029664.99615.94

Lucieer, A., Jong, S.M. de, Turner, D. (2014): Mapping landslide displacements using Structure from Motion (SfM) and image correlation of multi-temporal UAV photography. Progress in Physical Geography: Earth and Environment, 38, 97–116. https://doi.org/10.1177/0309133313515293

Luo, L., Ma, W., Zhang, Z., Zhuang, Y., Zhang, Y., Yang, J., Cao, X., Liang, S., Mu, Y. (2017): Freeze/Thaw-Induced Deformation Monitoring and Assessment of the Slope in Permafrost Based on Terrestrial Laser Scanner and GNSS. Remote Sensing, 9, 198. https://doi.org/10.3390/rs9030198

Marcelino, E.V., Formaggio, A.R., Maeda, E.E. (2009): Landslide inventory using image fusion techniques in Brazil. International Journal of Applied Earth Observation and Geoinformation, 11, 181–191. https://doi.org/10.1016/j.jag.2009.01.003

Marendic, A., Paar, R., Tomic, H., Roic, M., Krkac, M. (2017): Deformation monitoring of Kostanjek landslide in Croatia using multiple sensor networks and UAV, in: INGEO 2017 – 7th International Conference on Engineering Surveying.

Martha, T.R., Kerle, N., Jetten, V., Van Westen, C.J., Vinod Kumar, K. (2010): Landslide volumetric analysis using cartosat-1-derived DEMs. IEEE Geoscience and Remote Sensing Letters, 7, 582–586. https://doi.org/10.1109/LGRS.2010.2041895

Mesić Kiš, I. (2017): Contribution to the application and terminology of geostatistical mapping methods in Croatia – Universal Kriging. Rudarsko-Geolosko-Naftni Zbornik, 32, 31–35. https://doi.org/10.17794/rgn.2017.4.3

Metternicht, G., Hurni, L., Gogu, R. (2005): Remote sensing of landslides: An analysis of the potential contribution to geo-spatial systems for hazard assessment in mountainous environments. Remote Sensing of Environment, 98, 284–303. https://doi.org/10.1016/j.rse.2005.08.004

Meza, J., Marrugo, A.G., Sierra, E., Guerrero, M., Meneses, J., Romero, L.A. (2018): A Structure-from-Motion Pipeline for Topographic Reconstructions Using Unmanned Aerial Vehicles and Open Source Software, in: Communications in Computer and Information Science. pp. 213–225. https://doi.org/10.1007/978-3-319-98998-3_17

Mihalić Arbanas, S., Arbanas, Ž. (2014): Landslide mapping and monitoring : Review of conventional and advanced techniques, in: Symposium of Macedonian Association for Geotechnics. pp. 57–72.

Milec, K., Bačić, Ž., Premužić, M., Šugar, D. (2015): Testiranje BiHPOS VPSP i CROPOS VPPS servisa (*Testing of BiHPOS VPSP and CROPOS VPPS services*), in: III. Kongres o Katastru u BiH. (*in Croatian*)

Mondini, A. (2017): Measures of Spatial Autocorrelation Changes in Multitemporal SAR Images for Event Landslides Detection. Remote Sensing, 9, 554. https://doi.org/10.3390/rs9060554

Mondini, A.C., Guzzetti, F., Chang, K.-T., Monserrat, O., Martha, T.R., Manconi, A. (2021): Landslide failures detection and mapping using Synthetic Aperture Radar: Past, present and future. Earth-Science Reviews, 216, 103574. https://doi.org/10.1016/j.earscirev.2021.103574

Mondini, A.C., Guzzetti, F., Reichenbach, P., Rossi, M., Cardinali, M., Ardizzone, F. (2011): Semi-automatic recognition and mapping of rainfall induced shallow landslides using optical satellite images. Remote Sensing of Environment, 115, 1743–1757. https://doi.org/10.1016/j.rse.2011.03.006

Moritani, R., Kanai, S., Date, H., Niina, Y., Honma, R. (2020): Plausible reconstruction of an approximated mesh model for next-best view planning of SfM-MVS. The International Archives of the Photogrammetry, Remote Sensing and Spatial Information Sciences, XLIII-B2-2, 465–471. https://doi.org/10.5194/isprs-archives-XLIII-B2-2020-465-2020

Moritani, R., Kanai, S., Date, H., Niina, Y., Honma, R. (2019): Quality Prediction of Dense Points Generated by Structure from Motion for High-Quality and Efficient As-Is Model Reconstruction. The International Archives of the Photogrammetry, Remote Sensing and Spatial Information Sciences, XLII-2/W13, 95–101. https://doi.org/10.5194/isprs-archives-XLII-2-W13-95-2019

Muja, M., Lowe, D.G. (2009): Fast approximate nearest neighbors with automatic algorithm configuration, in: Proceedings of the Fourth International Conference on Computer Vision Theory and Applications. SciTePress – Science and and Technology Publications, pp. 331–340. https://doi.org/10.5220/0001787803310340

Nichol, J., Wong, M.S. (2005): Satellite remote sensing for detailed landslide inventories using change detection and image fusion. International Journal of Remote Sensing, 26, 1913–1926. https://doi.org/10.1080/01431160512331314047

Niethammer, U., James, M.R., Rothmund, S., Travelletti, J., Joswig, M. (2012): UAV-based remote sensing of the Super-Sauze landslide: Evaluation and results. Engineering Geology, 128, 2–11. https://doi.org/10.1016/j.enggeo.2011.03.012

Nikolakopoulos, K., Kavoura, K., Depountis, N., Kyriou, A., Argyropoulos, N., Koukouvelas, I., Sabatakakis, N. (2017): Preliminary results from active landslide monitoring using multidisciplinary surveys. European Journal of Remote Sensing, 50, 280–299. https://doi.org/10.1080/22797254.2017.1324741

Nikolakopoulos, K.G., Kavoura, K., Depountis, N., Argyropoulos, N., Koukouvelas, I., Sabatakakis, N. (2015): Active landslide monitoring using remote sensing data, GPS measurements and cameras on board UAV, in: Michel, U., Schulz, K., Ehlers, M., Nikolakopoulos, K.G., Civco, D. (Eds.), Earth Resources and Environmental Remote Sensing/GIS Applications VI. p. 96440E. https://doi.org/10.1117/12.2195394

Nourbakhshbeidokhti, S., Kinoshita, A., Chin, A., Florsheim, J. (2019): A Workflow to Estimate Topographic and Volumetric Changes and Errors in Channel Sedimentation after Disturbance. Remote Sensing, 11, 586. https://doi.org/10.3390/rs11050586

Oniga, V.-E., Breaban, A.-I., Pfeifer, N., Chirila, C. (2020): Determining the Suitable Number of Ground Control Points for UAS Images Georeferencing by Varying Number and Spatial Distribution. Remote Sensing, 12, 876. https://doi.org/10.3390/rs12050876

Oppikofer, T., Bunkholt, H.S.S., Fischer, L., Saintot, A., Hermanns, R.L., Carrea, D., Longchamp, C., Derron, M.H., Michoud, C., Jaboyedoff, M. (2012): Investigation and monitoring of rock slope instabilities in norway by terrestrial laser scanning. Landslides and Engineered Slopes: Protecting Society through, 2, 1235–1241.

Oppikofer, T., Jaboyedoff, M., Keusen, H.-R. (2008): Collapse at the eastern Eiger flank in the Swiss Alps. Nature Geoscience, 1, 531–535. https://doi.org/10.1038/ngeo258

Padró, J.C., Muñoz, F.J., Planas, J., Pons, X. (2019): Comparison of four UAV georeferencing methods for environmental monitoring purposes focusing on the combined use with airborne and satellite remote sensing platforms. International Journal of Applied Earth Observation and Geoinformation, 75, 130–140. https://doi.org/10.1016/j.jag.2018.10.018

Pajares, G. (2015): Overview and Current Status of Remote Sensing Applications Based on Unmanned Aerial Vehicles (UAVs). Photogrammetric Engineering & Remote Sensing, 81, 281–330. https://doi.org/10.14358/PERS.81.4.281

Park, Lee (2019): On the Use of Single-, Dual-, and Quad-Polarimetric SAR Observation for Landslide Detection. ISPRS International Journal of Geo-Information, 8, 384. https://doi.org/10.3390/ijgi8090384

Passalacqua, P., Belmont, P., Staley, D.M., Simley, J.D., Arrowsmith, J.R., Bode, C.A., Crosby, C., DeLong, S.B., Glenn, N.F., Kelly, S.A., Lague, D., Sangireddy, H., Schaffrath, K., Tarboton, D.G., Wasklewicz, T., Wheaton, J.M. (2015): Analyzing high resolution topography for advancing the understanding of mass and energy transfer through landscapes: A review. Earth-Science Reviews, 148, 174–193. https://doi.org/10.1016/j.earscirev.2015.05.012

Pebesma, E.J. (2004): Multivariable geostatistics in S: the gstat package. Computers & Geosciences, 30, 683–691. https://doi.org/10.1016/j.cageo.2004.03.012

Pebesma, E.J., Wesseling, C.G. (1998): Gstat: a program for geostatistical modelling, prediction and simulation. Computers & Geosciences, 24, 17–31. https://doi.org/10.1016/S0098-3004(97)00082-4

Peternel, T., Kumelj, Š., Oštir, K., Komac, M. (2017): Monitoring the Potoška planina landslide (NW Slovenia) using UAV photogrammetry and tachymetric measurements. Landslides, 14, 395–406. https://doi.org/10.1007/s10346-016-0759-6

Powers, P.S., Chiarle, M., Savage, W.Z. (1996): A digital photogrammetric method for measuring horizontal surficial movements on the Slumgullion earthflow, Hinsdale County, Colorado. Computers & Geosciences, 22, 651–663. https://doi.org/10.1016/0098-3004(96)00008-8

Qi, S., Zou, Y., Wu, F., Yan, C., Fan, J., Zang, M., Zhang, S., Wang, R. (2017): A Recognition and Geological Model of a Deep-Seated Ancient Landslide at a Reservoir under Construction. Remote Sensing, 9, 383. https://doi.org/10.3390/rs9040383

Remondino, F., El-Hakim, S. (2006): Image-based 3D Modelling: A Review. The Photogrammetric Record, 21, 269–291. https://doi.org/10.1111/j.1477-9730.2006.00383.x

Röder, M., Hill, S., Latifi, H. (2017): Best practice tutorial: Technical handling of the UAV "DJI Phantom 3 Professional" and processing of the acquired data.

Rublee, E., Rabaud, V., Konolige, K., Bradski, G. (2011): ORB: An efficient alternative to SIFT or SURF, in: 2011 International Conference on Computer Vision. IEEE, pp. 2564–2571. https://doi.org/10.1109/ICCV.2011.6126544

Sammut, C., Webb, G.I. (2017): Encyclopedia of Machine Learning and Data Mining. Springer US, Boston, MA. https://doi.org/10.1007/978-1-4899-7687-1

Schlögel, R., Thiebes, B., Mulas, M., Cuozzo, G., Notarnicola, C., Schneiderbauer, S., Crespi, M., Mazzoni, A., Mair, V., Corsini, A. (2017): Multi-Temporal X-Band Radar Interferometry Using Corner Reflectors: Application and Validation at the Corvara Landslide (Dolomites, Italy). Remote Sensing, 9, 739. https://doi.org/10.3390/rs9070739

Shah, R., Deshpande, A., Narayanan, P.J. (2015): Multistage SFM: A Coarse-to-Fine Approach for 3D Reconstruction. https://doi.org/10.48550/ARXIV.1512.06235

Simeoni, L., Ferro, E., Tombolato, S. (2015): Reliability of Field Measurements of Displacements in Two Cases of Viaduct-Extremely Slow Landslide Interactions, in: Engineering Geology for Society and Territory – Volume 2. Springer International Publishing, Cham, pp. 125–128. https://doi.org/10.1007/978-3-319-09057-3_11

Smith, M.W., Carrivick, J.L., Quincey, D.J. (2016): Structure from motion photogrammetry in physical geography. Progress in Physical Geography: Earth and Environment, 40, 247–275. https://doi.org/10.1177/0309133315615805

Snavely, N., Seitz, S.M., Szeliski, R. (2008): Modeling the World from Internet Photo Collections. International Journal of Computer Vision, 80, 189–210. https://doi.org/10.1007/s11263-007-0107-3

Spreafico, M.C., Perotti, L., Cervi, F., Bacenetti, M., Bitelli, G., Girelli, V.A., Mandanici, E., Tini, M.A., Borgatti, L. (2015): Terrestrial Remote Sensing techniques to complement conventional geomechanical surveys for the assessment of landslide hazard: The San Leo case study (Italy). European Journal of Remote Sensing, 48, 639–660. https://doi.org/10.5721/EuJRS20154835

Stumpf, A., Malet, J.P., Allemand, P., Pierrot-Deseilligny, M., Skupinski, G. (2015): Ground-based multi-view photogrammetry for the monitoring of landslide deformation and erosion. Geomorphology, 231, 130–145. https://doi.org/10.1016/j.geomorph.2014.10.039

Sui, L., Wang, X., Zhao, D., Qu, J. (2008): Application of 3D laser scanner for monitoring of landslide hazards. The International Archives of the Photogrammetry, Remote Sensing and Spatial Information Sciences, 37, 277–282.

Szeliski, R. (2011): Computer Vision, Media, Texts in Computer Science. Springer London, London. https://doi.org/10.1007/978-1-84882-935-0

Tang, Y., Guo, Z., Wu, L., Hong, B., Feng, W., Su, X., Li, Z., Zhu, Y. (2022): Assessing Debris Flow Risk at a Catchment Scale for an Economic Decision Based on the LiDAR DEM and Numerical Simulation. Frontiers in Earth Science, 10, 1–21. https://doi.org/10.3389/feart.2022.821735

Tanteri, L., Rossi, G., Tofani, V., Vannocci, P., Moretti, S., Casagli, N. (2017): Multitemporal UAV Survey for Mass Movement Detection and Monitoring, in: Mikos, M., Tiwari, B., Yin, Y., Sassa, K. (Eds.), Advancing Culture of Living with Landslides. Springer International Publishing, Cham, pp. 153–161. https://doi.org/10.1007/978-3-319-53498-5_18

Tarolli, P. (2014): High-resolution topography for understanding Earth surface processes: Opportunities and challenges. Geomorphology, 216, 295–312. https://doi.org/10.1016/j.geomorph.2014.03.008

Teza, G., Galgaro, A., Zaltron, N., Genevois, R. (2007): Terrestrial laser scanner to detect landslide displacement fields: a new approach. International Journal of Remote Sensing, 28, 3425–3446. https://doi.org/10.1080/01431160601024234

Thibbotuwawa, A., Bocewicz, G., Nielsen, P., Banaszak, Z. (2020): UAVs Fleet Mission Planning Subject to Weather Fore-Cast and Energy Consumption Constraints, Advances in Intelligent Systems and Computing. Springer International Publishing. https://doi.org/10.1007/978-3-030-23946-6_8

Triggs, B., McLauchlan, P.F., Hartley, R.I., Fitzgibbon, A.W. (2000): Bundle Adjustment — A Modern Synthesis, in: Triggs B., Zisserman A., Szeliski R. (Eds) Vision Algorithms: Theory and Practice. pp. 298–372. https://doi.org/10.1007/3-540-44480-7_21

Tsai, M., Chiang, K., Huang, Y. (2010): The development of a direct georeferencing ready UAV based photogrammetry platform. International Archives of the Photogrammetry, Remote Sensing and Spatial Information Sciences – ISPRS Archives, 38.

Tsai, Z.-X., You, G.J.Y., Lee, H.-Y., Chiu, Y.-J. (2012): Use of a total station to monitor post-failure sediment yields in landslide sites of the Shihmen reservoir watershed, Taiwan. Geomorphology, 139–140, 438–451. https://doi.org/10.1016/j.geomorph.2011.11.008

Turner, D., Lucieer, A., de Jong, S. (2015): Time Series Analysis of Landslide Dynamics Using an Unmanned Aerial Vehicle (UAV). Remote Sensing, 7, 1736–1757. https://doi.org/10.3390/rs70201736

Turner, D., Lucieer, A., Wallace, L. (2014): Direct Georeferencing of Ultrahigh-Resolution UAV Imagery. IEEE Transactions on Geoscience and Remote Sensing, 52, 2738–2745. https://doi.org/10.1109/TGRS.2013.2265295

Ullman, S. (1979): The Interpretation of Structure from Motion. Proceedings of the Royal Society of London, 203, 405–426.

van Veen, M., Hutchinson, D.J., Kromer, R., Lato, M., Edwards, T. (2017): Effects of sampling interval on the frequency – magnitude relationship of rockfalls detected from terrestrial laser scanning using semi-automated methods. Landslides, 14, 1579–1592. https://doi.org/10.1007/s10346-017-0801-3

Verhoeven, G., Doneus, M., Briese, C., Vermeulen, F. (2012): Mapping by matching: a computer vision-based approach to fast and accurate georeferencing of archaeological aerial photographs. Journal of Archaeological Science, 39, 2060–2070. https://doi.org/10.1016/j.jas.2012.02.022

Warrick, J.A., Ritchie, A.C., Adelman, G., Adelman, K., Limber, P.W. (2017): New Techniques to Measure Cliff Change from Historical Oblique Aerial Photographs and Structure-from-Motion Photogrammetry. Journal of Coastal Research, 33, 39–55. https://doi.org/10.2112/JCOASTRES-D-16-00095.1

Westoby, M.J., Brasington, J., Glasser, N.F., Hambrey, M.J., Reynolds, J.M. (2012): 'Structure-from-Motion' photogrammetry: A low-cost, effective tool for geoscience applications. Geomorphology, 179, 300–314. https://doi.org/10.1016/j.geomorph.2012.08.021

Wheaton, J.M., Brasington, J., Darby, S.E., Sear, D.A. (2009): Accounting for uncertainty in DEMs from repeat topographic surveys: improved sediment budgets. Earth Surface Processes and Landforms, 35, 136–156. https://doi.org/10.1002/esp.1886

Yang, Z., Li, Z., Zhu, J., Preusse, A., Yi, H., Hu, J., Feng, G., Papst, M. (2017): Retrieving 3-D Large Displacements of Mining Areas from a Single Amplitude Pair of SAR Using

Offset Tracking. Remote Sensing, 9, 338. https://doi.org/10.3390/rs9040338

Yu, X., Hyyppä, J., Karjalainen, M., Nurminen, K., Karila, K., Vastaranta, M., Kankare, V., Kaartinen, H., Holopainen, M., Honkavaara, E., Kukko, A., Jaakkola, A., Liang, X., Wang, Y., Hyyppä, H., Katoh, M. (2015): Comparison of Laser and Stereo Optical, SAR and InSAR Point Clouds from Air- and Space-Borne Sources in the Retrieval of Forest Inventory Attributes. Remote Sensing, 7, 15933–15954. https://doi.org/10.3390/rs71215809

Zhang, H., Aldana-Jague, E., Clapuyt, F., Wilken, F., Vanacker, V., Van Oost, K. (2019): Evaluating the potential of post-processing kinematic (PPK) georeferencing for UAV-based structure- from-motion (SfM) photogrammetry and surface change detection. Earth Surface Dynamics, 7, 807–827. https://doi.org/10.5194/esurf-7-807-2019

Zhao, C., Lu, Z. (2018): Remote Sensing of Landslides—A Review. Remote Sensing, 10, 279. https://doi.org/10.3390/rs10020279

URL 1: https://www.cropos.hr/servisi/vpps (accessed 17th March 2022)

URL 2: https://www.manualsdir.com/manuals/164878/leica-tps1200.html (accessed 11th May 2022)

URL 3: https://github.com/mapillary/OpenSfM (accessed 23rd September 2020)

URL 4: https://www.dji.com/hr/phantom-4-pro-v2/specs (accessed 16th April 2022)

URL 5: https://support.pix4d.com/hc/en-us/articles/202558679-Quality-report-specifications (accessed 10th March 2022)

URL 6: https://www.ugcs.com (accessed 12th February 2021)

SAŽETAK

Novi pristup praćenja pomaka klizišta pomoću bespilotnih fotogrametrijskih sustava

Klizišta predstavljaju velike opasnosti koje mogu uzrokovati katastrofalne ljudske žrtve te nanijeti veliku materijalnu štetu. Da bi se spriječile ili umanjile sve moguće posljedice koje klizišta prouzročuju, važno je poznavati kinematiku kretanja površinskih i podzemnih kliznih masa klizišta. Geodetske tehnike izmjere mogu se koristiti za potrebe praćenja te za izradu kinematičkoga modela klizišta. U današnje vrijeme jedna od najčešće korištenih geodetskih tehnika za potrebe praćenja klizišta jest fotogrametrijsko snimanje pomoću bespilotnih zrakoplovnih sustava. Rezultati su takvih snimanja gusti oblaci točaka, digitalni modeli terena te digitalne ortomozaik karte, a na temelju usporedbe tih rezultata u dvjema mjernim epohama mogu se odrediti pomaci klizišta. Ovaj rad predstavlja novu metodu obrade podataka s novim pristupom za određivanje pomaka klizišta na temelju podataka fotogrametrijskoga snimanja bespilotnim zrakoplovnim sustavima. Glavna je prednost nove metode u tome što ne zahtijeva izradu gustih oblaka točaka, digitalnih modela terena ili digitalnih ortomozaik karata za određivanje pomaka. Primjenjivost i točnost nove metode ispitane su na testnome polju sa simuliranim pomacima poznatih vrijednosti čiji su se iznosi kretali u rasponu od 20 do 40 cm u različitim smjerovima. Nova metoda uspješno je odredila te pomake s 3D točnošću od ±1,3 cm.

Ključne riječi:
klizište, praćenje klizišta, bespilotni zrakoplovni sustavi, struktura iz pokreta, fotogrametrija

Author's contribution

Ivan Jakopec (PhD. Student) created the concept of the manuscript, developed the methodology, collaborated on the data collection, processed all measurement data, carried out the analyses, and validation, presented and interpreted the results and wrote the original draft manuscript. **Ante Marendić** (PhD., Associate Professor) collaborated on the data collection, contributed to the methodology, interpreted the results, gave suggestions for the discussion and conclusion, and critically reviewed and edited the draft version of the manuscript. **Igor Grgac** (PhD.) developed the methodology, participated in data collection, analyses, and validation, collaborated in the writing process, and critically revised and edited the draft version of the manuscript.